Analytical Investigation of the Performance of Reinforced Concrete Panels with boundary elements Under Quasi-static and Blast Loading

Osama Elwan [(1)], Tarek El Hashimy [(2)], Marwan Shedid [(3)]

Abstract— A brief description of latest modeling techniques adopted to analyze steel reinforced concrete panels under blast loading analysis are summarized, and then a macro-modelling technique utilizing the OpenSees software embedded layered-shell element was utilized and verified against experimental data under both quasi-static loading and blast loading, then the utilized model was used to perform a parametric study of the behavior of reinforced concrete panels under both quasi-static and blast loading to reflect the effect of different boundary elements (BEs) configuration on the performance of those panels, after that, It was found that using boundary elements enhances the performance of reinforced concrete panels under such quasi-static loading nature by increasing the ultimate load capacity dramatically up to about 5 times the load capacity of a panel without boundary element. And this increase in load capacity is accompanied by a lower decrease in the ductility ratio to about half the panel without *BEs* due to the reduced ultimate displacements while using thick *BEs*. And then five blast scenarios were applied to control panel and five different panels with *BEs*, the applied 5 blast scenarios resulted in varying range of damage extent, based on the impulse and time of each wave, with maximum difference of the resulted performance in panel without *BEs* under the variation of the blast waves, while maintaining smaller differences with the addition of the *BEs* in the other panels.

Index Terms— Blast load, Reinforced concrete panels, boundary elements, Analytical modelling, Macro-modelling, OpenSees modelling, Parametric study, out of plane loading.

1 Introduction

Recently several experimental studies were carried out to investigate the behavior of rectangular panels under both quasistatic and blast load (Lou Chung et al. (2007) [1], Razaqpur et al. (2006) [2]), however, limited number of them discussed the influence of adding boundary element (*BEs*) to panels when subjected to out-of-plane loading with impulsive nature (i.e. blast loads).

Reinforced concrete panels with *BE*s (i.e., parts of the panel with extra confinement, longitudinal reinforcement and with either the same thickness of the overall panel or thickening of the concrete panel at this part) have been widely investigated as a seismic force resisting system as alternative to conventional reinforced concrete panels with rectangular cross sections. The introduction of the *BE*s enhances the panel's in-plane performance because of the confinement action of the horizontal steel ties within the *BEs*, which increase the latter's compressive strain capacity, and thus improve the overall panel performance.

Under blast load, the nature of rapid strains causes rapid stress variations within the panel, those generated stresses could exist within the elastic limit of the concrete and can surpass the elastic zone going through plastic nonlinear behavior, the resulted damage would depend on the ability of the concrete panel to perform beyond the elastic limit which is dependent on its ductility performance.

Analytical studies were developed in this study and were verified against the experimental studies under both quasi-static and blast loads to get reliable model that provides a better understanding of the actual behavior of panels under those types of loading.

The ductility and performance of a reinforced concrete panel depend on several factors, namely, the axial stresses acting on the cross-section of the panel (Su et al. [3], Shegay et al. [4], Alarcon et al. [5]), the steel reinforcement ratio (Lu et al. [6], Priestley et al. [7]), panel aspect ratio (Gullu et al. [8]), end support conditions (Doh et al. [9]), and the confinement of concrete, especially in *BEs* (Kim et al. [10]). In order to investigate the effect of the different aforementioned parameters, and to further understand the performance of reinforced concrete panels with BEs under both quasi-static and blast loading taking into consideration the rapid strain rate, an analytical model able to predict the out-of-plane behavior of concrete panels under such loads with reliable results for both elastic and inelastic behavior is needed.

Several finite element models have been introduced in the literature to predict the out-of-plane behavior of different panel types (i.e., with and without *BEs*). According to Cerioni and Donida (1994) [11] and Hallinan and Guan (2007) [12], layered elements are one of the most effective FE models that can account for both flexural and shear deformations. A layered-shell element model was recently utilized to simulate the out-of-plane response of unreinforced (Noor-E-Khuda et al. 2016) [13] and reinforced masonry walls (El-Hashimy et al. 2019) [14], and to simulate the in-plane performance of reinforced concrete shear walls (Lu et al. 2015) [15]. In the current study, the model was further extended to simulate the out-of-plane response of reinforced concrete panels when subjected to both quasi-static

- *(1) Demonstrator and MSc Candidate at faculty of engineering, Ain Shams University.*
- *(2) Associate Professor of Concrete structures at faculty of engineering, Ain Shams University.*
- *(3) Professor of Concrete structures at faculty of engineering, Ain Shams University.*

uniform load and blast load scenarios, in order to evaluate the effect of different parameters on the wall displacement response.

2 Development of Analytical Macro-Model

2.1 Model Description

Analytical model was developed to investigate the out-of-plane behavior of RC panels under both quasi-static and blast loading. Therefore, a macro analytical model using OpenSees software (Version 3.2.2) was developed. In this research, a review of the model components and the used materials are described and utilized with the case of reinforced concrete panels to account for the resulting nonlinear behavior and rapid strain effect under quasistatic and blast loads. Analytical results from the developed models are verified against previously published results in the literature.

2.2 Material models

Two primary material models are used to represent concrete and steel reinforcement. For the concrete material, Lu et al. (2015) [15] used a concrete model created specifically for the layered finite element method (LFEM) in OpenSees. This concrete model relies on the smeared crack approach, which incorporates damage mechanics theory. More specifically, once the panel's cracking limit is achieved, the damage model considers its material to be orthotropic. Following that, based on crack direction, the model applies directional damaging effects to the elastic constituent matrix. The crack band concept (Basant and Oh 1983) [16] used in the model, depicts fracture as a smeared crack band instead of a single crack. The tension strain inside the formed crack is subsequently diffused across a crack band width, and the tension stress-strain interaction is then governed by the cracking process, which includes tension softening (Rots 1988) [17]. To account for the effect of increased confinement stirrups in the BEs, both confined and unconfined concrete materials have been considered in the current study (i.e., increased ultimate strain and enhanced compressive strength).

In the models used for verification, the axial compressive strength, f_c, of the unconfined concrete material was taken equal to the reported values of the test specimens in each of the panels modeled , while the elastic modulus (E_c) and shear modulus (G) were determined as $4700\sqrt{(fc)}$ as per ACI (318-19) [18] and $Ec/(2(1+v))$ [19], respectively. Finally, the strain at ultimate compressive strength, ε_{cu}, was estimated to be 0.0025 for unconfined concrete based on stress-strain models reviewed by Samani et al. (2012) [20].

As previously stated, BEs, unlike the web component of the panel, utilize closed ties that provided confinement of concrete within the BE cores This confinement improves the strength and ductility of the concrete within the BEs and is modeled using Mander et al. (1988) [21] model to estimate the confined compressive strength, f_{cc}, and the corresponding compressive strain, ε_{ccu}.

Both the vertical and horizontal reinforcement bars are simulated in the LFEM as corresponding thicknesses of steel layers. The PlateRebar material model (featured in OpenSees) was utilized in this model. The yield strength of steel reinforcement, f_y, for each panel analyzed – in the models used for verification - was determined based on reported experimental tension testing results. Strain hardening ratio of (1%) was assumed (ratio between post-yield and initial elastic tangents (Filippou et al. 1983 [22]), while steel Young's modulus of 200 GPa was used in the model.

2.3 Geometry model

In order to model the concrete geometry of each panel, four-node multi-layer shell elements (SHELLMITC4 in OpenSees) (Lu et al. 2015) [15] was utilized as illustrated in Figure (1), the cross sections of these shell elements were divided into layers, with materials (i.e., Confined concrete, Unconfined concrete, horizontal and vertical reinforcement) assigned to various layers based on their respective place inside the panel as illustrated in Figure (2), to achieve equal strain distribution across both vertical and horizontal directions, the shell components were constrained to a square form (Bazant and Oh, 1983) [23].

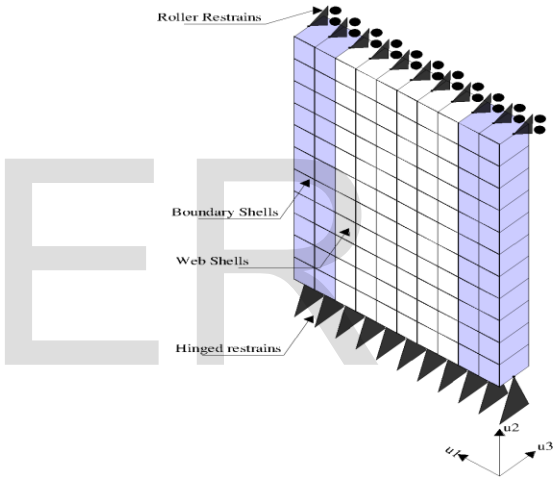

Fig. 1. Panel is divided into four-node multi-layer shell elements.

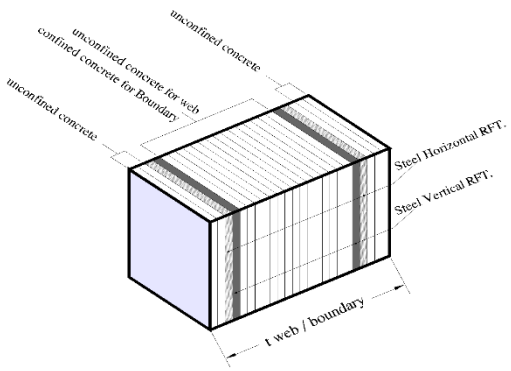

Fig. 2. the cross sections of each shell element separated into various layers.

2.4 Model Loads

Axial load on the panel due to gravity loads or even external applying loads has a considerable impact on the displacement ductility (defined as the ratio of the peak nonlinear displacement to the yield displacement) of load-bearing walls (e.g., Shedid et al. 2009; El-Hashimy et al. 2019) [24], [25]), vertical point loads were applied to the top of each node.

As for the quasi-static loading, displacement control static push over loading was carried out until the peak load capacity was achieved, and then the resulted load displacement resistance function was recorded to show the behavior of various panel under such load.

while for the blast loads, the pressure variation against time of the explosion front wave was idealized as exponential degradation function as presented in (USDOD 2008) [26] and based on Friedlander's Decay coefficients [27]. which were utilized to calculate the blast wave characteristics and pressure-time series. Fig (3) shows the idealized blast wave utilizing Friedlander equation [27]. Since the current study exclusively studies far-field explosion loading (i.e., scaled distance equal to or more than 1.2 m/kg$^{1/3}$ (ASCE 2011) [28] on individual components), the pressure distribution on the surrounding concrete panels was assumed to spread equally (ASCE 2011 [28]; USDOD 2008 [26]). Thus, the blast wave produced load that was uniformly applied on the panel surface in the out-of-plane direction.

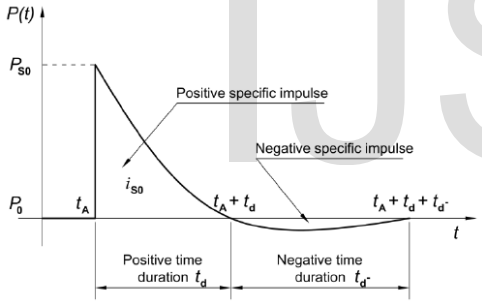

Fig. 3. The idealized waveform using the Friedlander equation [27].

2.5 Verification of Analytical Model Against Experimental Quasi-Static Test by Lou Chung et al. (2007):

The developed model was also validated based on the published results of Lou Chung et al. (2008) [1] where simply supported slabs were tested under four-point load configuration. The test specimen (S0-20-44) used for model validation was of 500 mm wide, 1200 mm long, and 90 mm thick slabs.

The chosen specimen was analyzed using the proposed finite element model under a displacement control static push overloading until the peak load capacity was reached. The resulted load displacement resistance function was compared against that of the experimental specimen as shown in Figure (4), and it is shown that the proposed finite element model resulted matching resistance function with the experimental curve where the deviation in the peak load was 6.82 % from the experimental corresponding load.

From another perspective, comparing the initial and post yield stiffness resulting from the model to the experimental curve we can see that both curves are fit and result in very close stiffnesses in both stages with deviations less than 5%. As for the yielding of reinforcement both analytical and experimental resistance functions conform matching results in both load and displacement values.

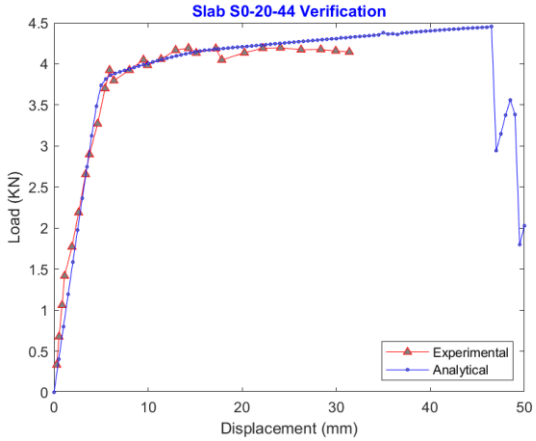

Fig. 4. Resistance function of experimental test versus the proposed analytical model.

2.6 Verification of Analytical Model Against Experimental Blast Tests by Razaqpur et al. (2006):

Razaqpur et al. [2] tested eight reinforced concrete panels in order to investigate their behavior under blast loading. Five panels were set as control panels, the geometry and reinforcement of control panels are shown in Figure (5). Steel mesh of designation MW 25.8 were used, which has bar cross-sectional area of 25.8 mm^2, mass per unit area of 2.91 kg/m^2 and center-to-center spacing of 152 mm in each direction. The bar yield stress and ultimate strength are 480 MPa and 600 MPa, respectively. The concrete had an average 28-day compressive strength of 40 MPa, with its average strength at the age of testing the panels being 42 MPa

The blast loads were produced by detonating either a 22.4 kg or a 33.4 kilograms ANFO (Ammonium Nitrate fuel oil) explosive charge at a 3-m standoff. Blast wave characteristics were measured in steel and concrete surfaces, including incident, and reflected pressures and impulses, as well as panel central deflection and strain in steel and on concrete surfaces were measured.

By comparing the peak displacement at the center of the panel from the analytical model to the experimental results, a max deviation of 12.21 % was observed as summarized in Table 1.

Furthermore, the resulted crack patterns in the experimental tests of panel CS2 were compared with the resulted analytical strains, it was observed that both analytical and experimental studies showed flexural behavior cracking pattern, and the strains in the analytical model expected almost identical

cracks to those results in the experimental tests as shown in Figure (6).

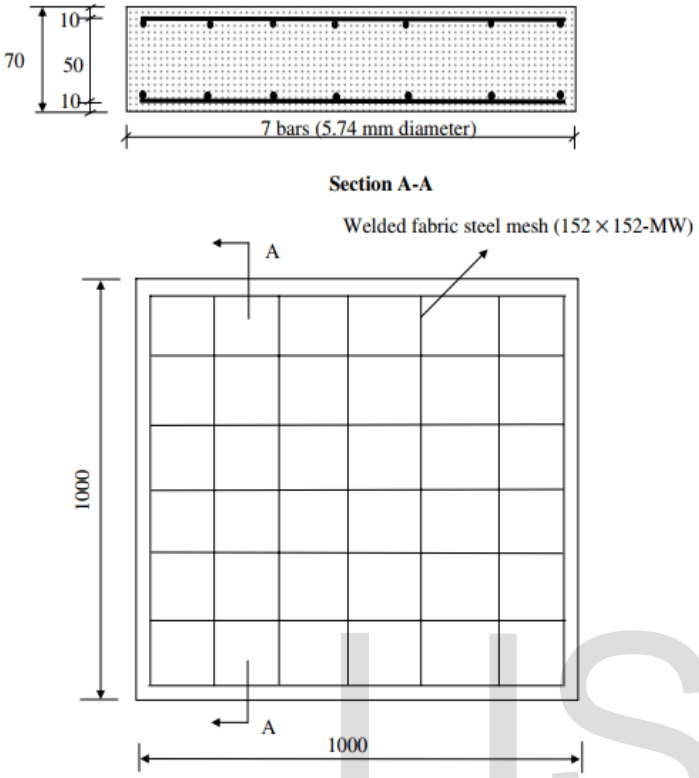

Fig. 5. Control panel geometry in mm and reinforcement (Razaqpur et al., 2006) [2].

TABLE 1
EXPERIMENTAL RESULTS VERSUS THE RESULTS OF THE PROPOSED ANALYTICAL MODEL OF PANELS CS1, CS2 AND CS3.

Panel	Reflected Pressure (Kpa)		Maximum experimental deflection (mm)	Maximum analytical deflection (mm)	Analytical Error %
	Max.	Ave.			
CS4	4823	3842	8.33	9.35	12.21%
CS2	5528	5059	13.12	13.91	5.99%
CS3	5712	5507	9.53	9.35	-1.90%

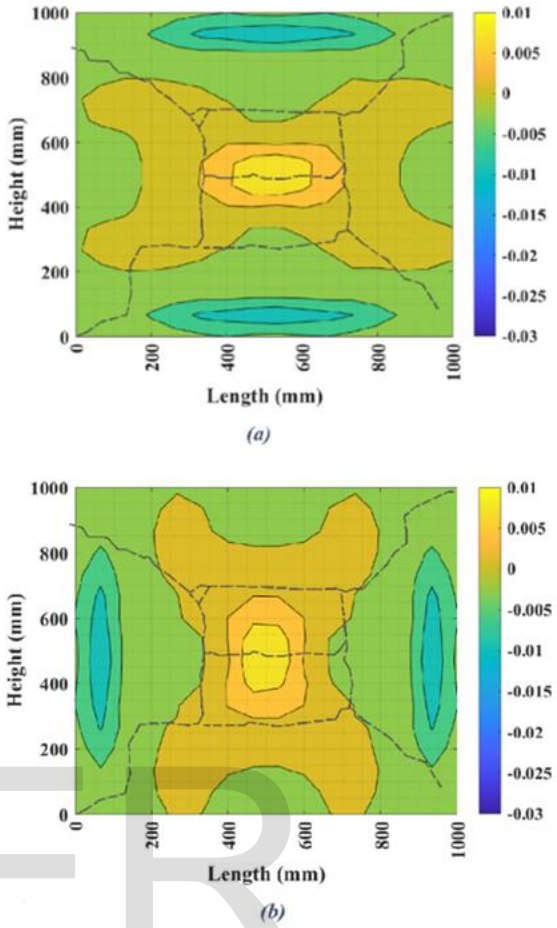

Fig. 6. (a) Vertical Strains (b) horizontal strains. Both recorded at extreme concrete fiber in tension side at the time of peak strain read versus the resulted cracks in experimental test as dash lines.

2.7 Model conclusion

A macro modelling technique was presented in this study that can model the quasi-static and dynamic behavior of the reinforced concrete panels and result in reliable structural behavior. This model was verified against both quasi-static and dynamic blast loadings, resulting in satisfying results with a maximum deviation in the displacement response of 6.82% and 12.21% from the published results of push over and experimental blast tests.

The adopted model will be used to conduct a parametric study and to well understand the performance of the reinforced concrete panels under such a load nature.

3 Effect of Boundary Elements on The Resistance function of Panels Under Quasi-Static Loading

In this first part of the parametric study, one control panel with rectangular section (W) and 15 other panels with *BEs* (BWs) are analyzed under quasi-static loading. The effect of different configurations using *BEs* on the resistance and ductility of the panels is studied. A detailed description of the panel properties and configurations are shown in Table (2) and figure (6). All panels are 3200 mm in height and width, while the web thickness is 250 mm. The vertical and horizontal reinforcement meshes consists of bars with 10 mm diameter every 200 mm and all *BEs* have stirrups with diameter of 10 mm every 200mm.

TABLE 2

SUMMARY OF THE GEOMETRIES OF THE TESTED PANELS UNDER QUASI-STATIC LOADING

Panel	t_{Flange} (mm)	A_{svb}
W	-----	-----
BW1-B25	250	8T16
BW1-B35	350	8T18
BW1-B50	500	10T18
BW2-B25	250	8T16
BW2-B25	350	8T18
BW2-B50	500	10T18
BW3-B25	250	8T16
BW3-B35	350	8T18
BW3-B50	500	10T18
BW4-B25	250	8T16
BW4-B35	350	8T18
BW4-B50	500	10T18
BW5-B25	250	8T16
BW5-B35	350	8T18
BW5-B50	500	10T18

All the modeled panels are restrained at the top and bottom edges of the panel while being free at the vertical edges. The bottom support of the panel restrains all three displacement degrees of freedom while the top support only restrains displacement in the out of plane direction. This choice of supporting condition is to prevent membrane action that occurs inside the panel and eliminate this beneficial action that is rare to exist in real life panels due to the fixation methods from the study results.

Figure (7) shows the configurations used in the study, the first type of panel is without any *BEs*, while the following five panels BW1 to BW5 are panels with *BEs* at different location, varying from one panel at the mid-web, two panels at either the extreme ends of the panel or at 0.2L from the far ends, panel with 3 BWs and with 4 BWs distributed at equal spacings. Those *BEs* vary in thickness from being embedded (with the same thickness of the web and with only extra stirrup confinement and concentrated reinforcement), to larger thicknesses of 350 and 500 mm.

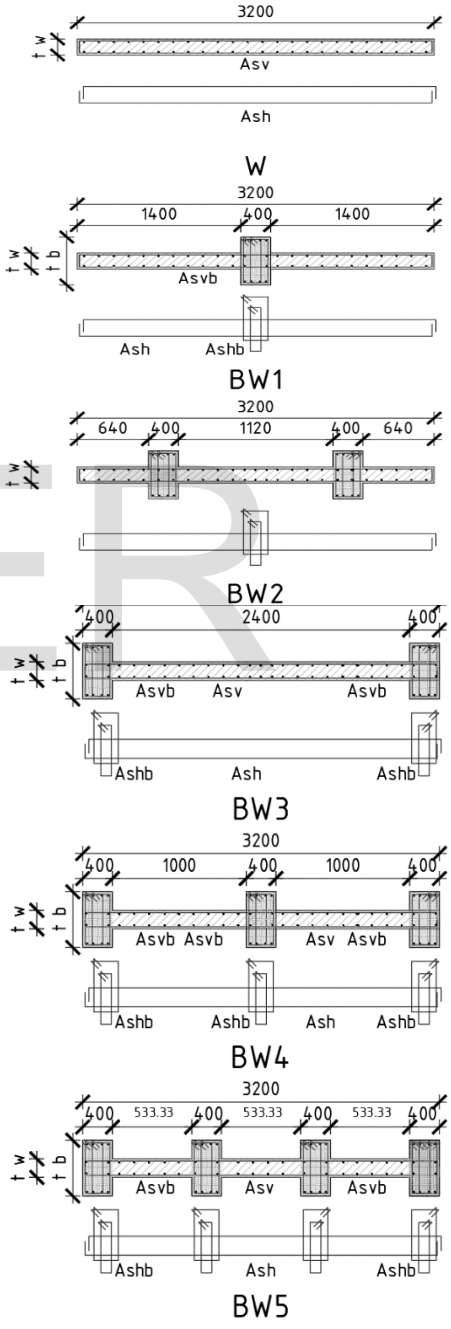

Fig. 7. The basic geometries of the 6 control panels adopted in this parametric study

Furthermore, the used material models for all panels have the same concrete compressive strength and steel yielding strength of 30 MPa and 450 MPa respectively. The effect of Confinement of concrete inside the stirrups of *BEs* is taken into consideration using Mander et al. (1988) stress-strain model [21].

Displacement control push-over loading analysis inside the OPENSEES software was adopted to generate the resistance function of each panel. The resistance functions are then idealized based on ASCE (41-13) [29] in order to estimate the panel achieved ductility. The influence of the BEs configurations is illustrated by comparing the resulted resistance functions as shown in figures (8) to (12).

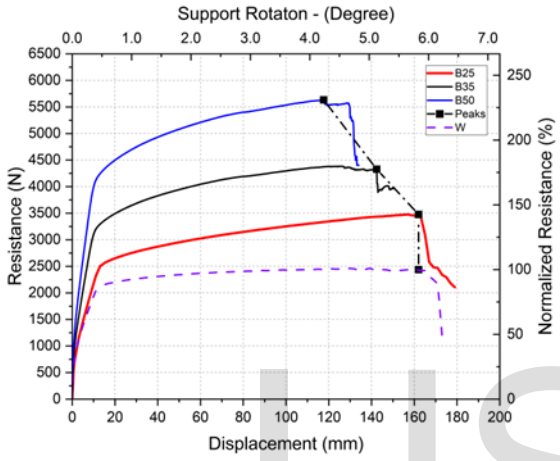

Fig. 8. Control Panel (W) against boundary arrangement of type (BW1)

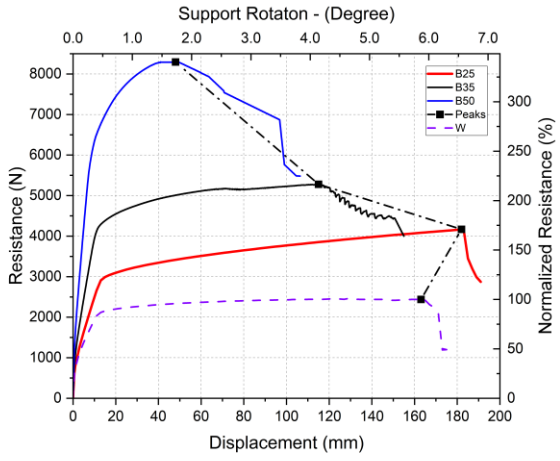

Fig. 9. Control Panel (W) against boundary arrangement of type (BW2)

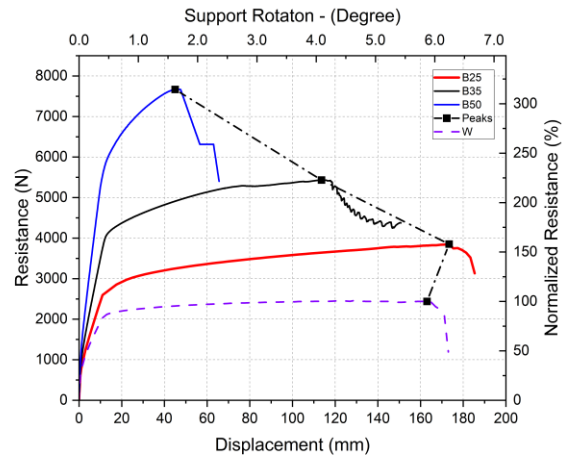

Fig. 10. Control Panel (W) against boundary arrangement of type (BW3)

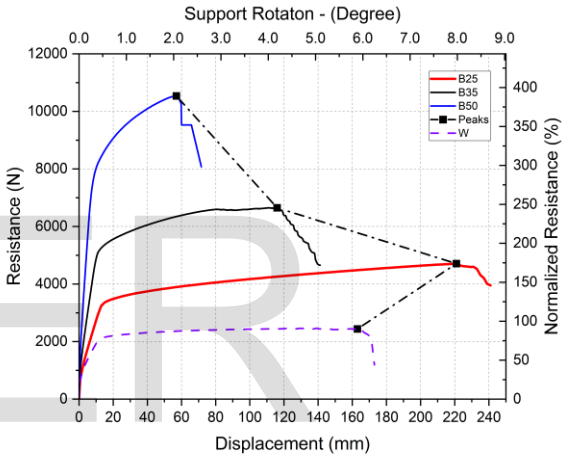

Fig. 11. Control Panel (W) against boundary arrangement of type (BW4)

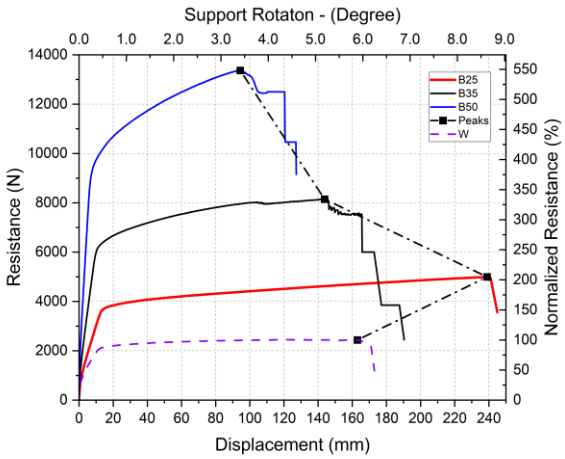

Fig. 12. Control Panel (W) against boundary arrangement of type (BW5)

Idealized resistance functions according to ASCE (41-13) [29] were generated, and then *Pu, Py, Δy* and *Δu* were calculated as defined in the ASCE (41-13) [29], Figure (13) shows the generated idealized resistance function versus the Analytical resistance function of control panel W.

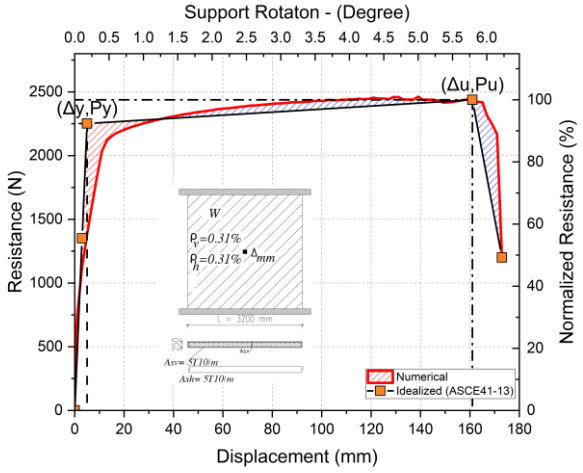

Fig. 13. Analytical resistance function versus the idealized resistance function according to ASCE (41-13) of panel W.

Results of this phase of the study were concluded and summarized in Fig. (14) and Table (3). The peak resistance of each panel and the achieved ductility are shown in Fig. (14) as normalized percentages with respect to the control panel (W). On the other hand, table (3) summarized the resulted yield and peak resistances, corresponding yield and peak displacements, the ductility ratio, and the normalized percentages of each panel with respect to the control panel (W).

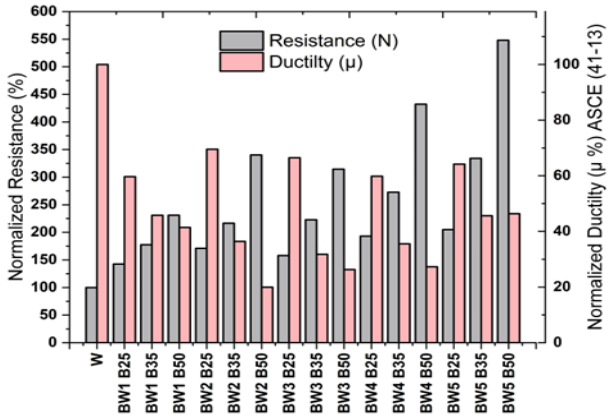

Fig. 14. Normalized Peak resistance and ductility ratio with respect to the control panel (W).

TABLE 3
SUMMARY OF QUASI-STATIC RESULTS.

Panel	Pu (N)	Pu (%)	Δ y (mm)	Δ u (mm)	μ	μ (%)
W	2438	100%	5.0	161	32.7	100 %
BW1 B25	3476	143%	8.3	157	19.5	60%
BW1 B35	4328	178%	9.7	142	15.0	46%
BW1 B50	5634	231%	9.0	118	13.6	41%
BW2 B25	4169	171%	8.3	183	22.7	70%
BW2 B35	5279	216%	10.3	115	11.9	36%
BW2 B50	8295	340%	7.7	41	6.5	20%
BW3 B25	3853	158%	8.3	173	21.7	66%
BW3 B35	5434	223%	12.0	114	10.4	32%
BW3 B50	7668	314%	10.3	45	8.6	26%
BW4 B25	4708	193%	11.7	221	19.6	60%
BW4 B35	6647	273%	10.3	111	11.6	36%
BW4 B50	10537	432%	7.3	57	8.9	27%
BW5 B25	4996	205%	11.7	239	21.0	64%
BW5 B35	8146	334%	10.0	144	14.9	46%
BW5 B50	13365	548%	6.7	94	15.2	46%

It can be observed that with respect to peak resistance, BW5 achieved the highest resistance for all of the boundary arrangement. As expected, the peak resistance increases as the number of *BEs* increases. As reported in table (3) for BW1-B50 up to BW5-B50. the normalized peak resistance was 231%, 340%, 314%, 432%, and 548% with respect to the control panel (W) respectively.

However, the contribution of the first added *BEs* at the middle of the panel width increased the peak resistance by 131%. Similarly, adding two and three *BEs* in BW2 and BW4 enhanced the peak resistance by 240% and 332% respectively. Thus, the contribution of each single BE decreases while increasing the number of BEs in the configuration (i.e., the peak resistance increase per boundary is reducing with more added *BEs*) this conclusion is valid on the other thicknesses of *BEs* as seen in Table (3).

for example, for BW1-B25 to BW1-B50, the normalized peak resistance values were 143%, 178%, and 231%. maintaining the same panel thickness while adding concentrated reinforcement with extra confining stirrups increase the peak resistance with

43%, while increasing the thickness of the *BEs* to 35 cm (40% more thick than 25cm) increased the load capacity with 78% (35% more than B25), and boundary of thickness 50 cm (100% thicker than 25 cm) increased the peak resistance with 131% (88% more than B25). From that we can conclude that *BEs* with 35 cm (1.4 web thickness) achieved enhanced performance while maintaining satisfying economic result with 40% only increase in boundary thickness compared to the web thickness.

From another perspective, it can be seen that adding *BEs* resulted in increased yielding displacement value while reducing the ultimate displacement value, consequently reducing ductility ratio compared to the control rectangular panel W. By comparing different BEs configurations (excluding the control panel (W)), it can be seen that for panels with embedded BEs, panel BW2 achieved the highest ductility ratio of 22.7, while with thick boundaries either with 35 cm or 50 cm boundary thickness, panel BW5 achieved the highest ductility rations of 14.9 and 15.2. These results can be interpreted as for boundary thicknesses 35 and 50 cm, BW5 achieved the highest ductility performance since it has the maximum number of BEs, resulting in the highest confinement, and with total steel to concrete percentages lower than the other type of panels. While under the embedded boundary case, the high concentration of reinforcement steel within thin concrete section resulted in postponing the yielding point of steel (High percentage of reinforcement), which lowered the calculated ductility ratio after BW2.

It can be summarized that using *BEs* enhances the performance of reinforced concrete panels under such quasi-static loading nature by increasing the peak resistance up to about 5 times the peak resistance of a panel without boundary element. This increase in resistance is accompanied by lower loss in the ductility performance (i.e., BW5 resistance ductility ratio was reduced by approximately 50%).

In addition to the conducted analysis on those panels under quasi-static loading, further investigation under blast waves is conducted in the following phase of this study.

4 Behavior of Panels with configurations of Boundary Elements Under Varying Blast Load

In this part of the study, five blast scenarios were generated under constant scaled distance (Z) of 1.75 m/kg $^{1/3}$ to ensure a far field effect and avoid the near field effects that are not to be considered in this study due to the limitations of used macro-modelling technique.

The characteristics of these five blast scenarios are detailed in Table (4), and the time history of those generated waves are plotted in figure (15) using Friedlander equation according to UFC (USDOD 2008) [26]. As simplification, the negative field pressure was neglected due to its minor influence on the structural component as stated in the literature (USDOD 2008) [26]. As seen from these characteristics that the key difference between these scenarios is the wave time and generated impulse, while keeping the peak reflected pressure constant as a result of the constant scaled distance value.

Different types of panels with the various *BEs* configurations from BW1 to BW5 and one control panel (*W*) as previously detailed in figure (7) with panel length and height of 3.2 meters and boundary element thickness of 350mm were analyzed under the generated blast scenarios, and the results were summarized in figure (16) and figure (17).

The peak displacements that took place for each panel were recorded in order to assess the level of damage of the different panels in accordance with the ASCE 59-11 [28]. As shown in figure (16), by applying the selected blast wave scenarios on the modeled aforementioned panels, the support rotation varies from 0.1 degree at scenario *BS1* a to a maximum of 5.8 degrees while applying scenario BS5. These support rotation values reflect the extent of occurring damage and the achieved level of performance (*LOP*) as mentioned in ASCE 59-11 (2011) [28]. Superficial damage will be expected at rotations below 2°, moderate damage will be the scenario around rotation values of 2°, while heavy and hazardous damage conditions will exist at rotations of 5° and 10°. The moderate damage LOP was highlighted on figure (16) by plotting a horizontal line corresponding to the support rotation of 2 degrees, it was noticed that at blast scenarios 1 and 2 all the analyzed panels had almost superficial to no damage, which can be seen from the slight support rotation values.

under blast scenario 3, the panels have support rotation values that range from 1.0 to 2.5 degrees, reflecting the moderate damage LOP and showing a difference of 1.5 degrees in support rotation from (BW5) to (W) panels.

Then when applying blast scenario 4 and 5, the panels have support rotation values that range from 1.5 to 5.8 degrees, reflecting the severe damage LOP and showing maximized differences in the performance between panels up to 3.8 degrees.

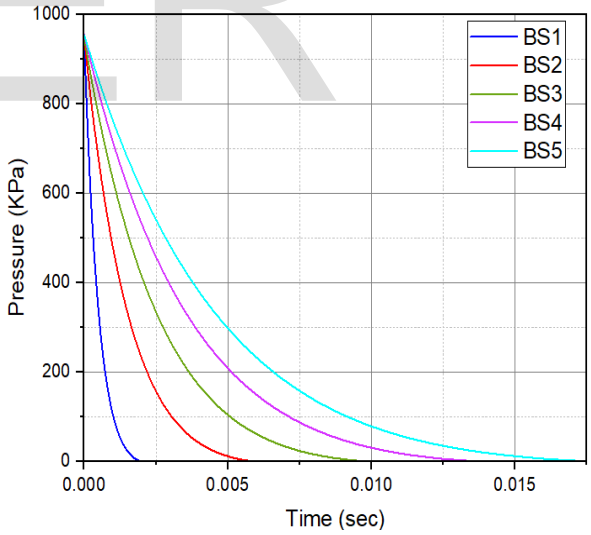

Fig. 15. The time history of the five applied blast scenarios BS1 to BS5

TABLE 4
SUMMARY OF BLAST SCENARIOS.

	BS1	BS2	BS3	BS4	BS5
W (Kg)	1.48	40	185	512	1088
R (m)	2	6	10	14	18
Z (m/kg 1/3)	1.75	1.75	1.75	1.75	1.75

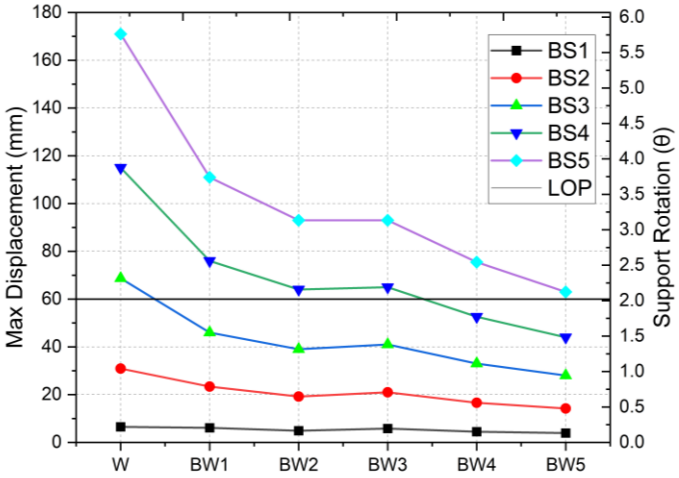

Fig. 16. Maximum displacement and support rotation of different panels under the varying blast scenarios showing the heavy damage LOP at corresponding to 2 degrees as per ASCE 59-11 [28].

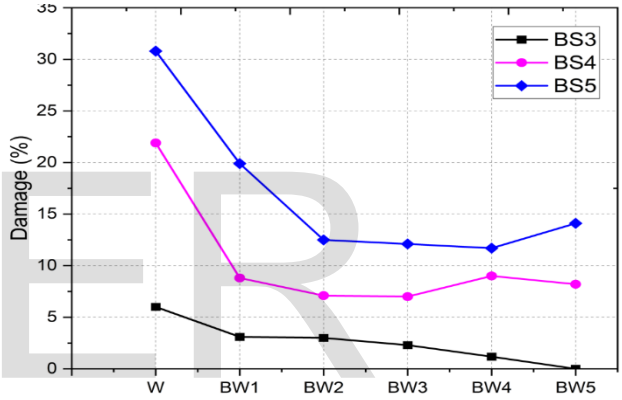

Fig. 17. Damage percent of different panels under the varying blast scenarios.

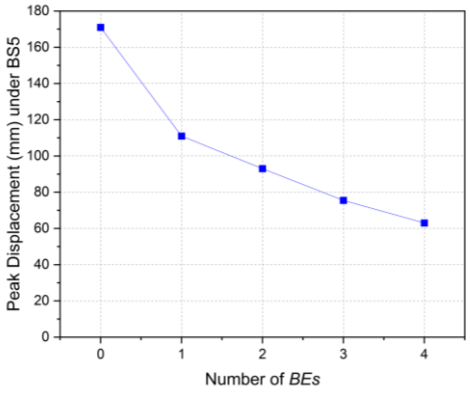

Fig. 18. Resulted peak displacement under BS5 versus the used number of *BEs*.

To monitor the performance of those panels by another aspect, damage percentages were recorded in each panel under different blast waves by determining the percentage of modeled shell elements that reached the ultimate concrete strain in the outer fibers reflecting the reached damage percentage and plotted in figure (17). Blast scenarios 1 and 2 were not shown in figure (17) since none of the analyzed panels show any damage.

Comparing the results of figure (17) which reflects the damage percentages as per the analytical model versus the results of figure (16) which shows the resulted peak displacement and the corresponding support rotation for each panel, and interpreting those support rotation values with the corresponding stated performance levels and states of damage as in the literature, we can see that both figure (16) or figure (17) show that all panels have superficial to no damage. While under blast scenarios 3, 4 and 5, the analyzed panels show moderate to heavy damage performance, which can be reflected either by the support rotation values in figure (16) of 1.5 to 5.8 degrees, or by the resulted damage percentages in figure (17) of 5% to 32%.

The differences between those panels at the maximum blast scenario 5 were compared to each other. Figure (18) shows the resulted peak displacement versus the number of the added BEs, the slope of the curve reflects the maximized effect of the first added *BE* reducing the peak displacement from 171 mm to 111 mm (35% reduction in peak displacement), while adding two or the *BEs* results in lower slope in the curve, the results are 93 mm (with two *BEs*), which means another 10.5% reduction for the second added *BE*, and 75.5 mm (with three *BEs*), which means another 10.2% reduction for the second added *BE*. The fourth added *BE* result in lower slope, achieving peak displacement of 63 mm, which means only 7.3% reduction for the fourth added *BE*.

Concluding, we can summarize that the applied 5 blast scenarios resulted in varying range of damage extent, based on the impulse and time of each wave, and highlighting that the effect of Panel configuration has a clear effect on the performance of each panel. The resulted peak displacement in each panel under different blast scenarios were summarized, and it was found the under same peak wave pressure while changing the impulse of waves, the analyzed panels undergo different levels of damage, and those damage levels were recorded either by the peak displacement and the corresponding support rotation, or with recording the number of shells exceeding the ultimate concrete strain in the compression fiber.

Under blast scenario 5 with the highest applying wave impulse and maximum difference between panels, it was shown that adding *BEs* to the panel enhanced the resulted performance, and this improvement result per added boundary element was maximized for the first added *BE,* and then lowered for the second and third added *BEs* with similar improvement values, while being minimized for the fourth added *BE*.

References

[1] Chung, Lou, Husam Najm, and Perumalsamy Balaguru. "Flexural behavior of concrete slabs with corroded bars." Cement and Concrete Composites 30.3 (2008): 184-193.

[2] Razaqpur, A. G., Tolba, A., & Contestabile, E. (2006, December 23). Blast loading response of reinforced concrete panels reinforced with externally bonded GFRP laminates. Composites Part B: Engineering.

[3] R.K.L. Su, S.M. Wong, Seismic behaviour of slender reinforced concrete shear walls under high axial load ratio, Engineering Structures, Volume 29, Issue 8, 2007, Pages 1957-1965, ISSN 0141-0296.Cerioni, R., and G. Donida. "A Finite Element Model for the Nonlinear Analysis of Reinforced and Prestressed Masonry Walls." Computers & Structures, vol. 53, no. 6, Dec. 1994, pp. 1291–1306, 10.1016/0045-7949(94)90397-2.

[4] Shegay, A. V., Motter, C. J., Elwood, K. J., Henry, R. S., Lehman, D. E., & Lowes, L. N. (2018). Impact of Axial Load on the Seismic Response of Rectangular Walls. Journal of Structural Engineering, 144(8).

[5] Alarcon, C., Hube, M. A., & de la Llera, J. C. (2014). Effect of axial loads in the seismic behavior of reinforced concrete walls with unconfined wall boundaries. Engineering Structures, 73, 13–23.

[6] Lu, Y., & Henry, R. S. (2017). Numerical modelling of reinforced concrete walls with minimum vertical reinforcement. Engineering Structures, 143, 330–345.

[7] Priestley, M. J. N., & Kowalsky, M. J. (1998). Aspects of drift and ductility capacity of rectangular cantilever structural walls. Bulletin of the New Zealand Society for Earthquake Engineering, 31(2), 73–85.

[8] Gullu, M. F., & Orakcal, K. (2019). Nonlinear Finite Element Modeling of Reinforced Concrete Walls with Varying Aspect Ratios. Journal of Earthquake Engineering, 1–32.

[9] Doh, J. H., Lee, D. J., Guan, H., & Loo, Y. C. (2008, May). Concrete wall with various support conditions. In Proceeding of the 4th International Conference on Advances in Structural Engineering and Mechanics (ASEM 08) (pp. 967-975).

[10] Kim, S.-H., Lee, E.-K., Kang, S.-M., Park, H.-G., & Park, J.-H. (2021). Effect of boundary confinement on ductility of RC walls. Engineering Structures, 230, 111695.

[11] Cerioni, R., & Donida, G. (1994). A finite element model for the nonlinear analysis of reinforced and prestressed masonry walls. Computers & Structures, 53(6), 1291–1306.

[12] Hallinan, Philip, and Hong Guan. "Layered Finite Element Analysis of One-Way and Two-Way Concrete Walls with Openings." Advances in Structural Engineering, vol. 10, no. 1, Feb. 2007, pp. 55–72, 10.1260/136943307780150850. Accessed 7 July 2022.

[13] Noor-E-Khuda, Sarkar, et al. "An Explicit Finite Element Modelling Method for Masonry Walls under Out-of-Plane Loading." Engineering Structures, vol. 113, no. 0141-0296, Apr. 2016, pp. 103–120, 10.1016/j.engstruct.2016.01.026. Accessed 16 July 2020.

[14] El-Hashimy, T., Ezzeldin, M., Tait, M., & El-Dakhakhni, W. (2019). Out-of-Plane Performance of Reinforced Masonry Shear Walls Constructed with Boundary Elements. Journal of Structural Engineering, 145(8), 04019073.

[15] Xinzheng Lu, Linlin Xie, Hong Guan, Yuli Huang, Xiao Lu, A shear wall element for nonlinear seismic analysis of super-tall buildings using OpenSees, Finite Elements in Analysis and Design, Volume 98, 2015, Pages 14-25.

[16] Bažant, Zdeněk P., and B. H. Oh. "Crack Band Theory for Fracture of Concrete — Northwestern Scholars." Northwestern Scholars, www.scholars.northwestern.edu, 20 Mar. 2016.

[17] Rots, J. G. Computational Modeling of Concrete Fracture | TU Delft Repositories.

[18] ACI Committee 318. Building Code Requirements for Structural Concrete:

(ACI 318-95); and Commentary (ACI 318R-95). Farmington Hills, MI: American Concrete Institute, 1995.

[19] Skrzypek, J., & Ganczarski, A. (2015). Mechanics of anisotropic materials. Springer.

[20] Samani, A. K., & Attard, M. M. (2012). A stress–strain model for uniaxial and confined concrete under compression. Engineering Structures, 41, 335–349..

[21] Mander, J. B., Priestley, M. J. N., & Park, R. (1988). Theoretical Stress-Strain Model for Confined Concrete. Journal of Structural Engineering, 114(8), 1804–1826.

[22] Filippou, Filip C., Egor Paul Popov, and Vitelmo Victorio Bertero. "Effects of bond deterioration on hysteretic behavior of reinforced concrete joints." (1983): 137-147.

[23] Bažant, Zdeněk P., and Byung H. Oh. "Crack band theory for fracture of concrete." Matériaux et construction 16.3 (1983): 155-177.

[24] Shedid, Marwan T., Wael W. El-Dakhakhni, and Robert G. Drysdale. "Behavior of fully grouted reinforced concrete masonry shear walls failing in flexure: Analysis." Engineering Structures 31.9 (2009): 2032-2044.

[25] El-Hashimy, Tarek, et al. "Out-of-plane performance of reinforced masonry shear walls constructed with boundary elements." Journal of Structural Engineering 145.8 (2019): 04019073.

[26] US Department of Defense (2008) Structures to resist the effects of accidental explosions. Report no. UFC 3-340-02, December. Washington, DC: Unified Facilities Criteria.

[27] Dewey, John M. "The shape of the blast wave: studies of the Friedlander equation." 21st international symposium on military aspects of blast and shock, Israel. 2010.

[28] American Society of Civil Engineers (ASCE) (2011) Blast protection of buildings. ASCE SEI 59-11.

[29] American Society of Civil Engineers. "Seismic evaluation and retrofit of existing buildings." American Society of Civil Engineers, 2014.